REGULAR ARTICLE

Stereo-dynamics study of O + HCl → OH + Cl reaction on the ^{3}A″, ^{3}A′, and ^{1}A′ states

Mei Hua Ge · Yu Jun Zheng

Abstract Using three accurate potential energy surfaces of the ^{3}A″, ^{3}A′, and ^{1}A′ states constructed recently, we present a quasi-classical trajectory (QCT) calculation for O + HCl $(v = 0, \ j = 0) \rightarrow$ OH + Cl reaction at the collision energies (E_{col}) of 14.0–20.0 kcal/mol. The three angular distribution functions—$P(\theta_r)$, $P(\varphi_r)$, and $P(\theta_r, \varphi_r)$, together with the four commonly used polarization-dependent differential cross-sections, $\frac{2\pi}{\sigma}\frac{d\sigma_{00}}{d\omega_t}$, $\frac{2\pi}{\sigma}\frac{d\sigma_{20}}{d\omega_t}$, $\frac{2\pi}{\sigma}\frac{d\sigma_{22+}}{d\omega_t}$, and $\frac{2\pi}{\sigma}\frac{d\sigma_{21-}}{d\omega_t}$ are exhibited to get an insight into the alignment and the orientation of the product OH radical. There is a similar behavior of the tendency scattering direction for the two triplet electronic states (^{3}A″ and ^{3}A′)—backward scattering dominates, however, forward scattering prevails for the case of ^{1}A′ state. Also, obvious differences have been found in the stereo-dynamical information, which reveals the influences of the potential energy surface and the collision energy. The degrees of polarization and the influence of the collision energy on the stereo-dynamics characters of the title reaction are both demonstrated in the order of ^{3}A′ > ^{3}A″ > ^{1}A′.

Keywords Quasi-classical trajectory · Stereo-dynamics · Distribution function · Alignment · Orientation

1 Introduction

In the recent decades, the reactions of halogen-containing molecules have been received considerable attention. Because of the important role in stratospheric chemistry,

M. H. Ge (✉) · Y. J. Zheng
School of Physics, Shandong University, Jinan 250100, China
e-mail: mhge@sdu.edu.cn

numerous experimental [1–11] and theoretical [12–48] investigations of O + HCl appeared. Any dynamical calculation must rely on a sufficiently accurate potential energy surface (PES), preferably of ab initio stem. Since the first ab inito calculations by Hirsch et al. [44] and Bruna et al. [45], enormous efforts have been spent on the construction of O + HCl PESs [15, 16, 22–24, 31, 35, 47, 48]. Most previous studies deal basically with the scalar properties, such as reaction probability, the integral cross-section, vibrational/rotational distributions, and branching ratio, etc. The vector properties could provide valuable information about the stereo-dynamics, for example, velocity and momentum vectors contain magnitudes related to the translational and rotational energies and well-defined directions as well [49–59]. With the development of polarized laser techniques, the measurement of the reagent/product alignment and orientation could be realized. However, to the author's best knowledge, few literatures were concerned with the study of the vector properties about the title reaction. Although there are two channels for O + HCl on ^{1}A′ state [31], we only study the following one–O + HCl → OH + Cl in order to compare with the results on ^{3}A″/^{3}A′ state.

In this paper, using the recent-developed ^{3}A″/^{3}A′ [48] and ^{1}A′ [31] PESs, we perform a quasi-classical computation on the O + HCl $(v = 0, \ j = 0) \rightarrow$ OH + Cl reaction so as to study the influence of the PESs and collision energies on the stereo-dynamics characters. The ^{3}A″ and ^{3}A′ states [48] are degenerated at collinear and asymptotic regions of configuration space, and the scaled reaction barrier height on ^{3}A″/^{3}A′ state is 10.60/13.77 kcal/mol. The potential energy surface for the ^{3}A″ state contains a fairly deep van der Waals well (with the scaled depth of −5.22 kcal/mol) on the product side of the reaction barrier at a rather sharp O–H–Cl angle (68.57°) and a shallow well (the scaled depth is −1.54 kcal/mol) on the reactant side at

collinear O–H–Cl geometry. The reaction on $^1A'$ state [31] proceeds without a barrier. $^1A'$ state has a deep well in bent geometry corresponding to stable HOCl molecule, and the well depth is −101.47 kcal/mol.

2 Methodology and computational details

The QCT method used is similar to that described in Refs. [53–56]. We use the center-of-mass (CM) frame with the reagent relative velocity vector **k** paralleling to the z-axis and xz plane containing the initial and final velocity vectors (**k** and **k'**) as the scattering plane. In the center-of-mass frame, θ_r and φ_r refer to the corresponding polar and azimuthal angles of the product rotational momentum **j'**, and $\omega_t = \theta_t$, φ_t, the coordinates of the unit vector $\hat{k}'$ along the direction of the product velocity **k'**.

The distribution function $P(\theta_r)$ describing the **k**-**j'** correlation could be written as

$$P(\theta_r) = \frac{1}{2}\sum_k (2k+1)a_0(k)P_k(\cos\theta_r), \qquad (1)$$

where the polarization parameter $a_0(k)$ is given by

$$a_0(k) = \int_0^\pi P(\theta_r)P_k(\cos\theta_r)\sin\theta_r d\theta_r = \langle P_k(\cos\theta_r)\rangle. \qquad (2)$$

The expanding coefficients $a_0(k)$ are called orientation (k is odd) or alignment (k is even) parameters. And $P(\theta_r)$ is expanded up to $k = 18$ in this work to ensure the convergent results.

The dihedral angular distribution of the **k**-**k'**-**j'** correlation is characterized by the angle φ_r. The distribution function $P(\varphi_r)$ could be expanded as a Fourier series

$$P(\varphi_r) = \frac{1}{2\pi}(1 + \sum_{even, n \geq 2} a_n \cos n\varphi_r + \sum_{odd, n \geq 1} b_n \sin n\varphi_r), \qquad (3)$$

with a_n and b_n given by

$$a_n = 2\langle \cos n\varphi_r\rangle, \qquad (4)$$
$$b_n = 2\langle \sin n\varphi_r\rangle. \qquad (5)$$

In this calculation, $P(\varphi_r)$ is expanded to $n = 24$ so as to ensure the convergence.

The joint probability density function of angles θ_r and φ_r, which determines the direction of **j'**, could be represented as follows.

$$P(\theta_r, \varphi_r) = \frac{1}{4\pi}\sum_{kq}(2k+1)a_q^k C_{kq}(\theta_r, \varphi_r)^*$$
$$= \frac{1}{4\pi}\sum_k \sum_{q \geq 0}\left[a_{q\pm}^k \cos q\varphi_r - a_{q\mp}^k i \sin q\varphi_r\right]C_{kq}(\theta_r, 0). \quad (6)$$

Here

$$a_{q\pm}^k = 2\langle C_{k|q|}(\theta_r, 0)\cos q\varphi_r\rangle \quad \text{if } k \text{ even}, \qquad (7)$$
$$a_{q\pm}^k = 2i\langle C_{k|q|}(\theta_r, 0)\sin q\varphi_r\rangle \quad \text{if } k \text{ odd}. \qquad (8)$$

$C_{kq}(\theta_r, \varphi_r)$ are modified spherical harmonics. In our calculation, $P(\theta_r, \varphi_r)$ is expanded to $k = 7$, which is sufficient for good convergence.

The full three-dimensional angular distribution associated with **k**-**k'**-**j'** correlation could be given as

$$P(\omega_t, \omega_r) = \sum_{kq}\frac{2k+1}{4\pi}\frac{1}{\sigma}\frac{d\sigma_{kq}}{d\omega_t}C_{kq}(\theta_r, \varphi_r)^*, \qquad (9)$$

where $\frac{1}{\sigma}\frac{d\sigma_{kq}}{d\omega_t}$ is a generalized polarization-dependent differential cross-section (PDDCS), and it could be written as the following form

$$\frac{1}{\sigma}\frac{d\sigma_{kq\pm}}{d\omega_t} = \sum_{k_1}\frac{2k_1+1}{4\pi}S_{kq\pm}^{k_1}C_{k_1-q}(\theta_t, 0), \qquad (10)$$

where $S_{kq\pm}^{k_1}$ is an expected value with its expression given via

$$S_{kq\pm}^{k_1} = \langle C_{k_1 q}(\theta_t, 0)C_{kq}(\theta_r, 0)\left[(-1)^q e^{iq\varphi_r} \pm e^{-iq\varphi_r}\right]\rangle. \quad (11)$$

The angular brackets $\langle \cdots \rangle$ in Eq. 11 represent the average over all angles.

The initial ro-vibrational numbers of the HCl reactant are chosen at $v = 0$, and $j = 0$ level, 10,000 trajectories are used on the three electronic states ($^3A''$, $^3A'$, and $^1A'$) over the collision energy range of 14.0–20.0 kcal/mol. The time integral step size and the energy gap are 10^{-4} ps and 1 kal/mol in due order.

3 Results and discussion

3.1 $P(\theta_r)$ distributions

On all three electronic states of $^3A''$, $^3A'$, and $^1A'$, $P(\theta_r)$ distributions are symmetric with respect to 90°, indicating that the product angular momentum **j'** tends to align along the direction perpendicular to initial velocity vector **k**. As described in Refs. [57, 58], $P(\theta_r)$ is sensitive to two factors: the characters of PESs and the mass factors. We use the same mass factor in our calculation. The distinct difference of $P(\theta_r)$ distributions on three different states probably comes from the different characteristics of the three PESs. Comparing all the $P(\theta_r)$ distributions generated on the three surfaces, one could clearly observe that products of $^3A'$ state display the strongest alignment for the highest and narrowest distribution, and next are those on $^3A''$ state, while those on $^1A'$ state show the least alignment for the lowest and broadest distribution. Over the
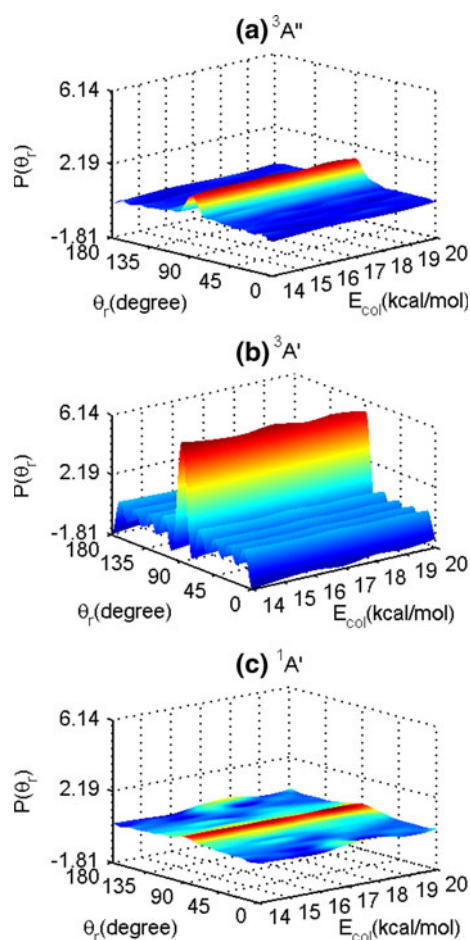
Fig. 1 The $P(\theta_r)$ distributions as a function of both the polar angle θ_r and the collision energy E_{col} for the O + HCl $(v = 0, j = 0) \rightarrow$ OH + Cl reaction on **a** $^3A''$, **b** $^3A'$, and **c** $^1A'$ states

Fig. 2 The $P(\varphi_r)$ distributions as a function of the dihedral angle φ_r at four collision energies of 14.0, 16.0, 18.0, and 20.0 kcal/mol (from inner to outer) for the O + HCl $(v = 0, j = 0) \rightarrow$ OH + Cl reaction on **a** $^3A''$, **b** $^3A'$, and **c** $^1A'$ states

whole collision energy range, different collision energies correspond to different alignment degrees. The $P(\theta_r)$ distributions do not contract or expand monotonously with the increase in E_{col}, which implies the higher collision energy does not definitely lead to the stronger product alignment. This is exhibited in Fig. 1. Apparently, the alignment degrees on the three electronic states are in the order of $^3A' > ^3A'' > ^1A'$. Usually, as well-known high barrier leads to strong rotational alignment/orientation. And deep well causes weak rotational alignment/orientation. Since a large number of resonances appear in reaction probabilities and the reaction is dominated by the formation of a complex due to the deep well. The complex-forming mechanism usually favors the molecule rotation in various directions so that the product alignment and orientation degree would be weak. For the two triplet states, the reaction barrier on $^3A'$ state is higher than the barrier on $^3A''$ state. There is no barrier on $^1A'$ state, but a much deeper well exists compared with the well depth on $^3A''$ state. This might give a reason of different polarization/

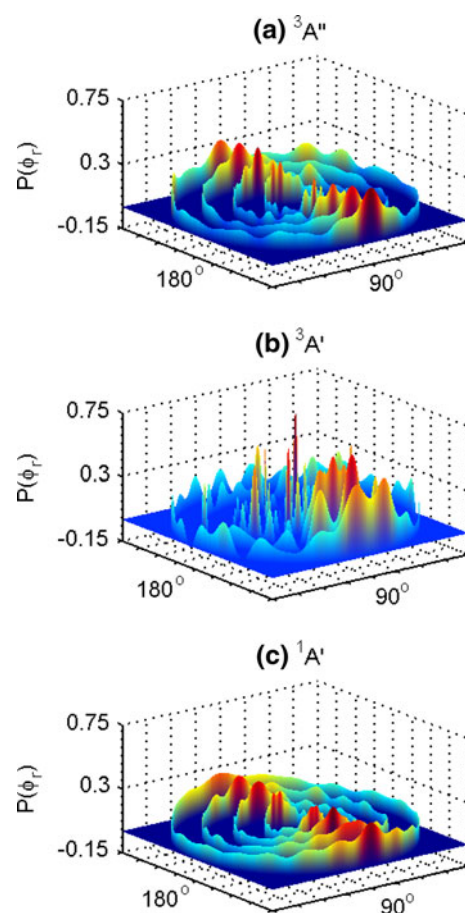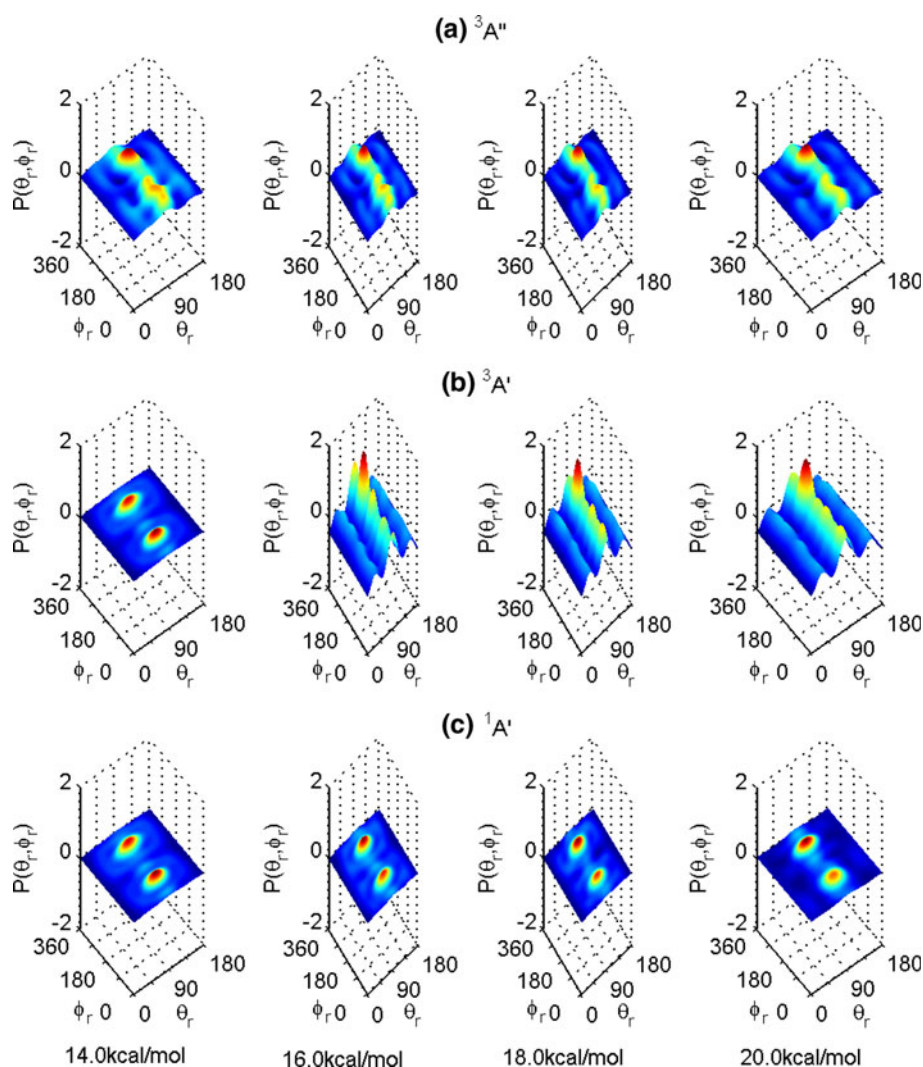orientation degrees on the three states, which will be also shown in Figs. 2, 3 and 4.

3.2 $P(\varphi_r)$ distributions

The $P(\varphi_r)$ distributions on the three electronic states at four collision energies (14.0, 16.0, 18.0, and 20.0 kcal/mol) are given in Fig. 2. Since φ_r is the dihedral angle between the planes consisting of **k**-**k′** (the scattering xz plane) and **k**-**j′**, $P(\varphi_r)$ function describes the **k**-**k′**-**j′** vector correlation and could provide some stereo-dynamical information on the alignment and orientation characters of the product as well. As shown in Fig. 2, all the values of $P(\varphi_r)$ are larger or equal to zero except for the case of $^3A'$ PES in Fig. 2b. We could also observe that the products formed on $^3A'$ PES have the strongest alignment and orientation, and those on $^3A''$ come second, while those on $^1A'$ are the least. All $P(\varphi_r)$ distributions tend to be asymmetric with respect to **k**-**k′** plane (the scattering xz plane), which directly reflects the strong polarization of product angular momentum **j′**. Besides the case of the low collision energy of 14.0 kcal/mol

on $^3A'$ PES (such an energy is approaching to the height of reaction barrier, which might give the explanation of the particularity), all the largest peaks of $P(\varphi_r)$ distributions exist at/around either $\varphi_r = 90°$ or $\varphi_r = 270°$, which demonstrates that $\mathbf{j}'$ is preferentially oriented along the positive or negative direction of y-axis (*i.e.*, the alignment is along y-axis), respectively. The rotation direction of the product is not isotropic. Collision energy has influences on the distribution function of $P(\varphi_r)$. The increasing energy leads to the variation of alignment and orientation degree and even the direction of orientation. It seems that on $^3A'$ state, the effects of collision energy on product polarization are the most prominent. Obviously, the $P(\varphi_r)$ distributions display strong dependent behaviors not only on PESs, but also on collision energies.

3.3 Joint $P(\theta_r, \varphi_r)$ distribution

In order to further verify the above-mentioned findings associated with the influences of potential energy surfaces

and collision energies on the $P(\theta_r)$ and $P(\varphi_r)$ distributions, we also plot the joint $P(\theta_r, \varphi_r)$ distributions with peaks and valleys as displayed in Fig. 3. The joint $P(\theta_r, \varphi_r)$ distributions performed on $^3A'$ state in Fig. 3b show the most sensitive dependence on the collision energy, which could be observed prominently on the angular distributions in Figs. 1 and 2.

3.4 PDDCSs

The four commonly polarization-dependent differential cross-sections (PDDCSs): $\frac{2\pi}{\sigma} \frac{d\sigma_{00}}{d\omega_t}$, $\frac{2\pi}{\sigma} \frac{d\sigma_{20}}{d\omega_t}$, $\frac{2\pi}{\sigma} \frac{d\sigma_{22+}}{d\omega_t}$, and $\frac{2\pi}{\sigma} \frac{d\sigma_{21-}}{d\omega_t}$ as a function of both collision energy E_{col} and scattering angle (the angle between the reagent relative velocity $\mathbf{k}$ and the product velocity $\mathbf{k}'$) θ_t are exhibited in Fig. 4. A high sensitivity of PDDCSs to the potential energy surface could be easily observed.

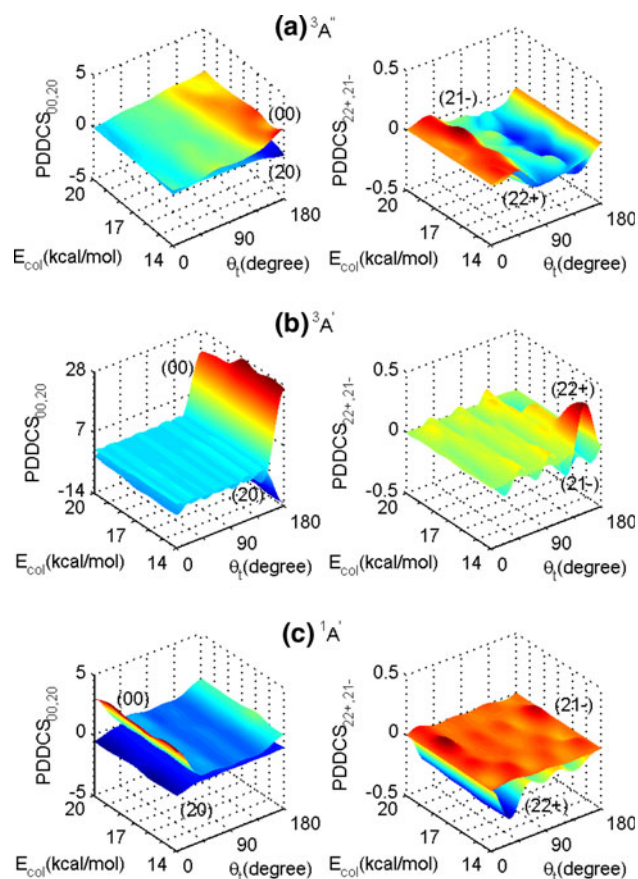As well known, $PDDCS_{00}$ is associated with the usual differential cross-sections, $PDDCS_{20}$ (alignment parameter),

Fig. 4 The PDDCSs (PDDCS$_{00}$, PDDCS$_{20}$, PDDCS$_{22+}$, PDDCS$_{21-}$) as a function of both the scattering angle θ_t and collision energy E$_{col}$ on **a** ^{3}A″, **b** ^{3}A′, and **c** ^{1}A′ surfaces

the expectation value of the second Legendre moment $\langle P_2(\cos \theta_r)\rangle$, PDDCS$_{22+}$, a reflection of the tendency alignment direction with the value of $\langle \sin^2 \theta_r \cos 2\varphi_r \rangle$, and PDDCS$_{21-}$ is similar with PDDCS$_{22+}$ with the value of $\langle -\sin 2\theta_r \cos \varphi_r \rangle$.

The PDDCS$_{00}$s of the two triplet states (^{3}A″ and ^{3}A′) show very strong backward scattering, while those of the singlet state (^{1}A′) demonstrate strong tendency of forward scattering. The variation laws and the magnitudes of PDDCS$_{00}$ with the increase in scattering angles on ^{3}A′ and ^{1}A′ surfaces are similar at different collision energies, and the only exception is 20.0 kcal/mol on ^{3}A′ surface. Although the varying collision energy does not change the scattering direction, it affects the magnitude of PDDCS$_{00}$. And on ^{3}A′ state, the influence of scattering angle on PDDCS$_{00}$ is the largest.

The PDDCS$_{20}$s on ^{3}A″ PES are close to -0.5 with the scattering angle around 150° at low collision energies (E$_{col}$ < 17.0 kcal/mol), which suggests that **j**′ is preferentially polarized perpendicular to the reagent velocity under such condition. While the angular momentum **j**′ is preferentially vertical polarized (**j**′⊥**k**) at very small scattering angles

(less than 10°) on ^{1}A′, and such polarization of **j**′ arises regardless of backward or forward scattering on ^{3}A′. At low collision energies (E$_{col}$ < 18.0 kcal/mol), the PDDCS$_{20}$s on ^{3}A′ PES are close to 1.0 when the scattering angles are about 8°, 135°, and 147°. This indicates that the angular momentum **j**′ is preferentially parallel or anti-parallel to the reagent relative velocity (**k**) on ^{3}A′ state under such conditions. But no such phenomena occur on ^{3}A″ and ^{1}A′ PESs. The relative high reaction barrier and deep well structure on ^{3}A′ PES might answer for its particularities. Moreover, as depicted in Figs. 1 and 2, on the three electronic states, the dependence of PDDCS$_{20}$ on collision energy is not a linear relationship. And the dependence of PDDCS$_{20}$ on collision energy is the least/most for ^{1}A′/^{3}A′ state, which is in agreement with the distributions of $P(\theta_r)$.

The positive value of PDDCS$_{22+}$ reveals the product alignment along x-axis. Conversely, the alignment is along y-axis. And the larger absolute value suggests the stronger alignment along the relevant axis. Moreover, if the value is close to zero, there is no obvious alignment direction. For ^{3}A″ and ^{1}A′ states, one could find that the product alignment is along y-axis at the overwhelming number of scattering angles, which also could be observed through the $P(\varphi_r)$ distributions in Fig. 2. For ^{1}A′/^{3}A″ state, alignment at small/large scattering angles is much stronger. For the ^{3}A′ electronic state, however, the alignment is either along x or along y-axis with the variation of the scattering angle. Through comparison, we conclude that ^{3}A′ PES shows the strongest alignment except for several medium collision energies, which agrees with the above description of the $P(\varphi_r)$ distributions. The dependence behavior on collision energy is the most/least prominent on ^{3}A′/^{1}A′ state, which also agrees with the case of the $P(\varphi_r)$ distribution functions.

According to the value of PDDCS$_{21-}$, one could clearly distinguish whether the product is aligned along the direction of vector **x** − **z** or **x** + **z**. For ^{3}A″ state, negative PDDCS$_{21-}$ values appearing at scattering angles larger or equal to 61° ($\theta_t \geq 61°$) indicate that the product alignment is along the direction of vector **x** + **z** at the overwhelming number of scattering angles, and the product alignment is along vector **x**–**z** since the values of PDDCS$_{21-}$ are smaller than zero at small scattering angles. For the case of ^{3}A′/^{1}A′ state, the alignment along **x** + **z** alternating with the alignment along **x** − **z** appears with the increase in scattering angle. And the values of PDDCS$_{21-}$ alternating negative positive with the variation of scattering angle are almost a process of synchronization for different collision energies on ^{3}A′ state.

4 Summary

We perform a quasi-classical dynamical calculation to study the stereo-dynamics information of the title reaction

on three different potential energy surfaces. We find the large influence of the potential energy surface on the stereo-dynamical characters. According to $P(\theta_r)$, $P(\varphi_r)$ and $P(\theta_r, \varphi_r)$ distributions and PDDCS$_{22+}$, one could conclude that the degrees of polarization are in the order of $^3A' > {}^3A'' > {}^1A'$, which are similar with the results of H/D + FO → OH/OD + F and HF/DF + O reactions [59]. The highest/no barrier on $^3A'/^1A'$ state and the deepest/no well on $^1A'/^3A'$ state might give an explanation of the interesting features. On the three potential energy surfaces, all the products are aligned perpendicular to the initial velocity vector according to the $P(\theta_r)$ distributions. The PDDCS$_{00}$ on the three states demonstrates different scattering behaviors—for the two triplet states ($^3A''$ and $^3A'$), backward scattering prevails, while for $^1A'$ state forward scattering dominates, and some information about the alignment direction and degree is also shown through PDDCS$_{20}$, PDDCS$_{22+}$, and PDDCS$_{21-}$. Moreover, the influences of the collision energy on the stereo-dynamics characters of the title reaction are exhibited in the order of $^3A' > {}^3A'' > {}^1A'$. We assume that the highest/no reaction barrier and no/the deepest well structure on $^3A'/^1A'$ state might give an explanation of their particularities.

References

1. Basco N, Norrish RGW (1961) Proc R Soc London Ser A 260:293–303
2. Luntz AC (1980) J Chem Phys 73:5393–5395
3. Rakestraw DJ, McKendrick KG, Zare RN (1987) J Chem Phys 87:7341–7342
4. Kruus EJ, Niefer BI, Sloan JJ (1988) J Chem Phys 88:985–992
5. Park CR, Wiesenfeld JR (1989) Chem Phys Lett 163:230–236
6. Balucani N, Beneventi L, Casavecchia P, Volpi GG (1991) Chem Phys Lett 180:34–40
7. Zhang R, van der Zande WJ, Bronikowski MJ, Zare RN (1991) J Chem Phys 94:2704–2712
8. Matsumi Y, Tonokura K, Kawasaki M, Tsuji K, Obi K (1993) J Chem Phys 98:8330–8336
9. Matsumi Y, Shamsuddin SM (1995) J Chem Phys 103:4490–4495
10. Alexander AJ, Brouard M, Rayner SP, Simons JP (1996) Chem Phys 207:215–226
11. Kohguchi H, Suzuki T (2006) Chem Phys Chem 7:1250–1257
12. Persky A, Broida M (1984) J Chem Phys 81:4352–4362
13. Schinke R (1984) J Chem Phys 80:5510–5517
14. Laganà A, de Aspuru GO, Gracia E (1995) J Phys Chem 99:17139–17144
15. Hernández ML, Redondo C, Laganà A, de Aspuru GO, Rosi M, Sgamellotti A (1996) J Chem Phys 105:2710–2718
16. Skokov S, Peterson KA, Bowman JM (1998) J Chem Phys 109:2662–2671
17. Alvariño JM, Bolloni A, Hernández ML, Laganà A (1998) J Phys Chem A 102:10199–10203
18. Poirier B (1998) J Chem Phys 108:5216–5224
19. Skokov S, Qi J, Bowman JM, Yang C-Y, Gray SK, Peterson KA, Mandelshtam VA (1998) J Chem Phys 109:10273–10283
20. Alvariño JM, Rodríguez A, Laganà A, Hernández ML (1999) Chem Phys Lett 313:299–306
21. Ramachandran B, Schrader EA III, Senekowitsch J, Wyatt RE (1999) J Chem Phys 111:3862–3873
22. Peterson KA, Skokov S, Bowman JM (1999) J Chem Phys 111:7446–7456
23. Christoffel KM, Kim Y, Skokov S, Bowman JM, Gray SK (1999) Chem Phys Lett 315:275–281
24. Matínez T, Hernández ML, Alvariño JM, Laganà A, Aoiz FJ, Menéndez M, Verdasco E (2000) Phys Chem Chem Phys 2:589–597
25. Lin SY, Han KL, Zhang JZH (2000) Phys Chem Chem Phys 2:2529–2534
26. Lin SY, Han KL, Zhang JZH (2000) Chem Phys Lett 324:122–126
27. Ramachandran B (2000) J Chem Phys 112:3680–3688
28. Bittererová M, Bowman JM (2000) J Chem Phys 113:1–3
29. Skokov S, Tsuchida T, Nanbu S, Bowman JM, Gray SK (2000) J Chem Phys 113:227–236
30. Nobusada K, Nakamura H, Lin Y, Ramachandran B (2000) J Chem Phys 113:1018–1026
31. Bittererová M, Bowman JM, Peterson K (2000) J Chem Phys 113:6186–6196 and references therein
32. Piermarini V, Balint-Kurti GG, Gray SK, Göğtas F, Laganà A, Hernández ML (2001) J Phys Chem A 105:5743–5750
33. Piermarini V, Lagana A, Balint-Kurti GG (2001) Phys Chem Chem Phys 3:4515–4521
34. Skokov S, Zou S, Bowman JM, Allison TC, Truhlar DG, Lin Y, Ramachandran B, Garrett BC, Lynch BJ (2001) J Phys Chem A 105:2298–2307
35. Christoffel KM, Bowman JM (2002) J Chem Phys 116:4842–4846
36. Nanbu S, Aoyagi M, Kamisaka H, Nakamura H, Bian W, Tanaka K (2002) J Theor Comput Chem 1:263–273
37. Kamisaka H, Nakamura H, Nanbu S, Aoyagi M, Bian W, Tanaka K (2002) J Theor Comput Chem 1:275–284
38. Kamisaka H, Nakamura H, Nanbu S, Aoyagi M, Bian W, Tanaka K (2002) J Theor Comput Chem 1:285–293
39. Lin SY, Park SC (2002) Bull Korean Chem Soc 23:229–240
40. Göğtas F, Bulut N, Akpinar S (2003) J Mol Struct (THEOCHEM) 625:177–187
41. Martínez T, Hernández ML, Alvariño JM, Aoiz FJ, Rábanos VS (2003) J Chem Phys 119:7871–7886
42. Bian W, Poirier B (2004) J Chem Phys 121:4467–4478
43. Yang H, Han KL, Nanbu S, Nakamura H, Balint-Kurti GG, Zhang H, Smith SC, Hankel M (2008) J Chem Phys 128:014308 (1–5)
44. Wei Q, Wu VWK (2009) Mol Phys 107:1453–1456
45. Hirsch G, Bruna PJ, Peyerimhoff SD, Buenker RJ (1977) Chem Phys Lett 52:442–448
46. Bruna PJ, Hirsch G, Peyerimhoff SD, Buenker RJ (1979) Can J Chem 57:1839–1851
47. Hauschildt J, Weis J, Beck C, Grebenschikov SY, Düren R, Schinke R, Koput J (1999) Chem Phys Lett 300:569–576
48. Ramachandran B, Peterson KA (2003) J Chem Phys 119:9590–9600 and references therein
49. Aoiz FJ, Bañares L, Herrero VJ (1998) J Chem Soc. Faraday Trans 94:2483–2500
50. de Miranda MP, Aoiz FJ, Bañares L, Sáez-Rábanos V (1999) J Chem Phys 111:5368–5383
51. de Miranda MP, Pogrebnya SK, Clary DC (1999) Faraday Discuss 113:119–132

52. Aldegunde J, de Miranda MP, Haigh JM, Kendrick BK, Sáez-Rábanos V, Aoiz FJ (2005) J Phys Chem A 109:6200–6217
53. Han KL, Zheng XG, Sun BF, He GZ, Zhang RQ (1991) Chem Phys Lett 181:474–478
54. Li RJ, Han KL, Li FE, Lu RC, He GZ, Lou NQ (1994) Chem Phys Lett 220:281–285
55. Han KL, He GZ, Lou NQ (1996) J Chem Phys 105:8699–8704 and references therein
56. Zhang X, Han KL (2006) Inter J Quant Chem 106:1815–1819
57. Wang ML, Han KL, He GZ (1998) J Chem Phys 109:5446–5454
58. Wang ML, Han KL, He GZ (1998) J Phys Chem A 102:10204–10210
59. Chu TS (2010) J Comput Chem 31:1385–1396